International journal of basic and applied research
www.pragatipublication.com
ISSN 2249-3352 (P) 2278-0505 (E)
Cosmos Impact Factor-5.86

EXPLORING THE SUPRAMOLECULAR ARCHITECTURE AND MULTIFUNCTIONAL PROPERTIES OF RUTHENIUM (II) POLYPYRIDYL COMPLEXES

[1]Dr N. Prashanthi, M.Sc, Ph.D, Assistant Professor, Department of Environmental Science, Pragati Engineering College.

[2]Jyotsna Akumuri, M.Sc, (Ph.D), Research Scholar, Department of Chemistry, Acharya Nagarjuna University, Guntur.

ABSTRACT:

Recent years have seen a considerable increase in interest in ruthenium(II) polypyridyl complexes because of their distinctive photophysical characteristics and possible biological uses. We investigate the supramolecular architecture of these complexes in this work in an effort to clarify the connection between their structural characteristics and multifunctional attributes. We have created a number of Ruthenium(II) polypyridyl complexes with different coordination environments and ligands by using a variety of synthetic techniques. Utilizing sophisticated spectroscopic methods such as time-resolved fluorescence spectroscopy, photoluminescence, and UV-Vis absorption, the supra molecular assembly of these complexes was examined. Important insights into the electronic transitions and excited-state dynamics of the compounds were obtained from these investigations. We also looked at their biological characteristics, paying particular attention to cytotoxicity, cellular absorption, and affinity for DNA binding. Our results show that the photophysical behavior and biological activity of Ruthenium(II) polypyridyl complexes are significantly influenced by their supra molecular architecture. Complexes with certain ligand configurations showed greater contacts with biological targets and improved photo stability, indicating that they might be useful as molecular probes and in photodynamic treatment. This study provides fresh insights into the potential uses of supra molecular design in the synthesis of multifunctional metal complexes in materials science and medicine. The findings provide for a better comprehension of the complicated interplay between structure and function in Ruthenium(II) polypyridyl complexes, which will facilitate the development of more potent medicinal compounds and imaging technologies.

I. INTRODUCTION

Deoxyribonucleic acid (DNA) is the primary carrier of all genetic information and it plays a major role in replication and storage of genes. Thus the molecules that interact with DNA have a variety of applications including pharmaceuticals, tools for molecular biology and probes for electron transfer.1,2 In this context, over the last two decades the transition metal polypyridyl complexes have received a considerable amount of attention.3–12 In particular coordinatively saturated ruthenium(II) polypyridyl complexes have received much attention because of their tuneable photophysical and photochemical properties, leading to a wide range of successful or potential applications in the

International journal of basic and applied research
www.pragatipublication.com
ISSN 2249-3352 (P) 2278-0505 (E)
Cosmos Impact Factor-5.86

field of photochemistry, photo-physics, and biochemistry.4,5,13,14 A widely studied [Ru(bpy)3] 2+ (bpy = 2,20 -bipyridine) complex binds electrostatically to DNA having binding affinity in the order of 103 M1 , 15 but when one of the bpy ligands is replaced with a dppz (dppz = dipyrido[3,2-a:20 ,30 -c]phenazine) ligand, it results in the [Ru(bpy)2(dppz)]2+ complex that binds intercalatively to DNA with a binding constant of the order 106 M1 and this complex also behaves as a molecular light switch for DNA.2,16,17 This shows that the DNA interaction properties of complexes can be tuned by modification of ligands. Ruthenium polypyridyl complexes interact with DNA by non-covalent interaction such as electrostatic, minor groove, major groove, partial intercalative and intercalative binding modes.18 However, there is still uncertainty on the exact location of binding modes. Further studies are necessary using different structural ligands to evaluate and understand the factors that determine the DNA binding modes.

It has been largely accepted that ruthenium(II) polypyridyl complexes can be used as probes for DNA structure determination,5,19,20,21 DNA photo-cleavage agents and DNA mediated electron transfer.13,22 Recent reports on advantages of ruthenium complexes as potential cellular imaging and anticancer agents has drawn much attention.4,5,20–36 In this context, recently Liang-Nian Ji and co-workers have reported the effect of hydrophobicity and the surface area of the ancillary ligands on the DNA binding and cytotoxicity properties of ruthenium complexes.31–34 More recently, J. Thomas and co-workers36 have reported the successful application of a dinuclear ruthenium(II) polypyridyl 'light switch' complex as an in cellulo nuclear stain, well tolerated by eukaryotic and prokaryotic cells. These results show that versatility of these complexes can be modified by the ligand set, which controls whether the complex is an intercalator, hemiintercalator or electrostatic binder.

As part of a project aimed at systematic structural alteration with a view to elucidating structure–activity relationships, here we report the synthesis, characterization, structural properties, DNA binding, DNA cleavage and preliminary anticancer activity of new complexes of the type [Ru(N–N)2(tdzp)]Cl2, where N–N is 2,20 -bipyridine (bpy) (1), 1,10-phenanthroline (phen) (2), dipyrido [3,2-d:20 ,3f] quinoxaline (dpq) (3), which incorporate [1,2,5]- thiadiazolo-[3,4-f]-[1,10]-phenanthroline (tdzp) (Scheme 1) as the ancillary ligand. Interestingly, complex 2 acts as a building block, generating a supramolecular framework encapsulating a cyclic hybrid chloride–water cluster {[(H2O)10(Cl)2] 2}n.

II. RESULTS AND DISCUSSIONS

Synthesis and characterization

[1,2,5]-Thiadiazolo-[3,4-f]-[1,10]-phenanthroline (tdzp) was synthesized as per literature procedure in four steps.37,38 The ruthenium(II) polypyridyl complexes of the type [Ru(N–N)2(tdzp)]2+ (1–3) (where, NN = bpy, phen, dpq) were synthesized by refluxing a 1 : 1 molar ratio of cis-[Ru(NN)2Cl2] and the [1,2,5]-thiadiazolo- [3,4-f]-[1,10]-phenanthroline (tdzp) ligand in methanol water mixture (1 : 1). The complexes obtained were purified

International journal of basic and applied research
www.pragatipublication.com
ISSN 2249-3352 (P) 2278-0505 (E)
Cosmos Impact Factor-5.86

by column chromatography using an activated neutral alumina column and obtained as racemic mixtures. The complexes were characterized by 1 H NMR, 13C NMR, IR, elemental analysis, UV-Visible spectroscopy and electrospray mass spectrometry (see the Experimental section). In ESI-MS peaks due to [M–Cl]+ and [M–2Cl]2+ were observed. The further physio-chemical and biological studies were carried out using the racemic mixtures.

Crystal structure of 210H2O. Crystals of complex 210H2O suitable for single crystal X-ray structure determination were grown by slow evaporation of solution of complex 2 in water :methanol

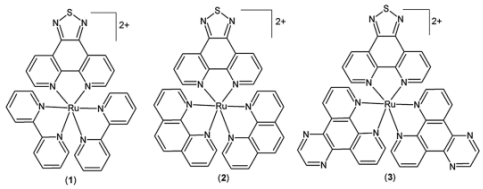

Scheme 1 Molecular structures of complexes 1–3.

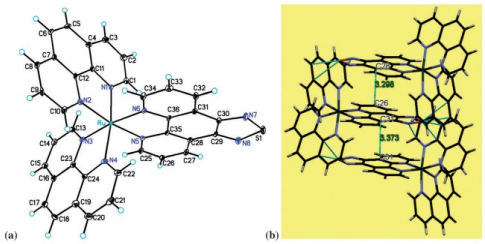

Fig. 1 (a) ORTEP diagram of the cation of 2, anions and solvent molecules were omitted for clarity, (b) pi–pi aromatic stacking interactions between planar tdzp ligands in 2. Selected bond lengths (Å): Ru–N1 = 2.060(5); Ru–N2 = 2.066(5); Ru–N3 = 2.054(5); Ru–N4 = 2.062(5); Ru–N5 = 2.053(5); Ru–N6 = 2.071(5). Selected bond angles (1): N(1)–Ru–N(2) = 79.80(2); N(3)–Ru–N(4) = 79.80(2); N(5)–Ru–N(6) = 79.95(2).

mixture at room temperature. An ORTEP diagram of cation of complex 2 is given in Fig. 1a. The complex crystallizes in the triclinic space group P1. Relevant crystallographic information % for complex 2 is given in Table S1 (ESI†), and a list of selected bond lengths and angles can be found in Table S2 (ESI†). The complex 2 crystallizes with ten water molecules and the two chloride anions were disordered over three positions. The ruthenium(II) was chelated by one tdzp ligand and two phenanthroline ligands. The coordination geometry around the ruthenium centre can be described as distorted octahedral, with an average bite angle of 79.85(2)1 between three polypyridyl ligands. The average Ru–N (1,10-phenatroline) bond length is 2.060(5) Å and Ru–N (tdzp) bond length is 2.061(5) Å, which is similar to the reported analogues mix ligand ruthenium(II) polypyridyl complexes.39–43 The crystal structure exhibits p–p aromatic stacking interactions involving a planar tdzp ligand with an inter-planar distance of 3.373 Å (C28–C26)/3.298 Å (C31–C31) (Fig. 1b).

Supramolecular architecture of 210H2O containing cyclic hybrid water–chloride cluster. Hydrated halide anions are an extremely active area of research, because they are the most common anions in nature due to their role in many chemical, environmental, and biological processes.44,45 Further studies on structures of halide–water clusters in nature is of fundamental importance for the understanding of the water–halide interaction in the atmosphere, ocean and biological systems.44,46,47 In particular,

International journal of basic and applied research
www.pragatipublication.com
ISSN 2249-3352 (P) 2278-0505 (E)
Cosmos Impact Factor-5.86

water–chloride interactions is one of the most commonly found interactions in nature (e.g., seawater or sea-salt aerosols), and thus the examination of water–chloride interactions has been the object of numerous theoretical studies.

Table 1 Selected hydrogen-bonding parameters[a]

D–H···A	D–H (Å)	H···A (Å)	D···A (Å)	D–H···A (°)
C1–H1···Cl2	0.95	2.67	3.431(7)	138.0
C9–H9···O3W^{i}	0.95	2.46	3.405(9)	170.8
C10–H10···O6W^{i}	0.95	2.45	3.236(9)	140.1
C21–H21···Cl2^{i}	0.95	2.87	3.815(7)	175.9
C25–H25···O1W^{ii}	0.95	2.55	3.326(10)	138.5
C26–H26···Cl3	0.95	2.73	3.676(7)	178.0
O1W–H1W1···Cl1	0.82(2)	2.33(3)	3.121(8)	164(10)
O1W–H1W2···S1^{iii}	0.82(2)	2.82(4)	3.620(9)	166(10)
O2W–H2W2···Cl3	0.83(2)	2.21(9)	2.876(12)	137(11)
O3W–H3W1···Cl1	0.82(2)	2.24(2)	3.056(7)	176(8)
O3W–H3W2···O7W^{iv}	0.81(2)	2.01(2)	2.815(8)	172(6)
O4W–H4W1···Cl1	0.84(2)	2.32(3)	3.147(8)	169(9)
O4W–H4W2···O2W^{v}	0.83(2)	2.03(4)	2.812(15)	157(8)
O5W–H5W1···O1W^{ii}	0.82(2)	2.14(2)	2.951(10)	174(7)
O5W–H5W2···O7W	0.81(2)	2.14(4)	2.863(8)	148(8)
O6W–H6W1···O3W	0.82(2)	2.03(2)	2.842(8)	173(6)
O6W–H6W2···O8W	0.81(2)	1.99(2)	2.803(9)	177(6)
O7W–H7W1···O9W	0.82(2)	2.00(5)	2.711(8)	144(8)
O7W–H7W2···O6W	0.82(2)	1.90(2)	2.718(8)	177(6)
O8W–H8W1···O4W	0.82(2)	2.08(7)	2.712(10)	134(9)
O8W–H8W2···O6W	0.81(2)	2.34(9)	2.803(9)	117(8)
O9W–H9W1···Cl1^{ii}	0.84(2)	2.33(7)	3.073(7)	147(11)
O9W–H9W2···O7W	0.83(2)	1.90(2)	2.711(8)	168(8)
O10W–H101···O8W	0.81(2)	2.01(5)	2.751(9)	153(9)
O10W–H102···Cl2	0.82(2)	2.27(3)	3.060(9)	164(9)

a Symmetry code(s): (i) x, y + 1, z; (ii) x + 1, y, z; (iii) x + 1, y + 1, z + 1; (iv) x + 1, y, z + 2; (v) x 1, y, z.

Recently several water chloride clusters in various crystal systems have been identified and structurally characterized.44,48,51 such as {[(H2O)20(Cl)4] 4}n, 48 [(H2O)6(Cl)2] 2, 51 [(H2O)10(Cl)2] 2. 44 These investigations are believed to provide an input towards the understanding of the hydration phenomena of chloride anions in nature and have importance in supramolecular chemistry, catalysis, biochemistry.

Interestingly in the crystal structure of 2 extensive hydrogen bonding interactions are observed between the all lattice water molecules and chloride anions (Table 1) leading to the formation

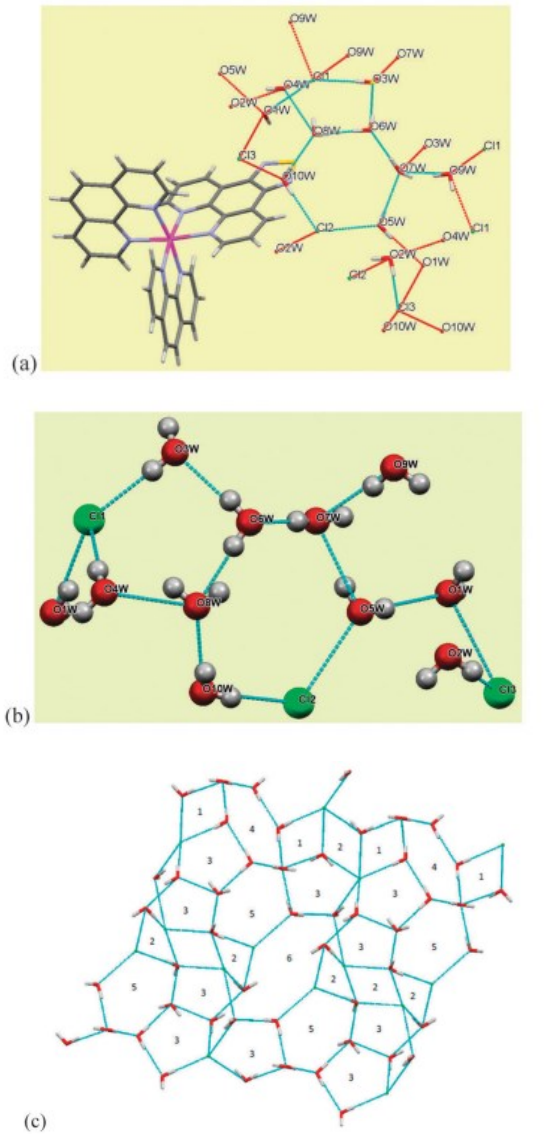

Fig. 2 (a) Ru(II) cationic building block 2 showing (arbitrary view) hydrogen bonding interactions between chloride anions and water molecules, (b) a closer view of the cyclic water–chloride cluster in 2, (c) nonplanar 2D anionic layer (arbitrary view) generated by the water–chloride cluster {[(H2O)10Cl2] 2}n.

International journal of basic and applied research
www.pragatipublication.com
ISSN 2249-3352 (P) 2278-0505 (E)
Cosmos Impact Factor-5.86

of a polymeric hybrid cyclic water–chloride cluster possessing minimal repeating {[(H2O)10(Cl)2] 2}n units (Fig. 2). The arrangement of atoms in the cyclic water–chloride cluster along with a proper atom labelling scheme is shown in Fig. 2. Each cyclic cluster consists of two chloride and ten water molecules, is connected to the next cyclic unit by the tail, having one water molecule. These clusters further interconnected by hydrogen bonding leading to a non-polar 2D water–chloride anionic layer (Fig. 2c). A packing diagram of 2 shows the arrangement of cationic molecules with tdzp ligands face to face by p–p stacking with the formation of channels encapsulating 2D water–chloride clusters. The space fill model of crystal packing of 2 view down the 'c' axis (Fig. 3 and Fig. S7, ESI†) shows that a 2D anionic hybrid water–chloride cluster {[(H2O)10(Cl)2] 2}n occupies the free space between hydrophobic arrays of the metal–organic part, with an inter layer separation of 11.907 Å which is equal to the b unit cell dimension (Table S1, ESI†). Nevertheless seven weak C–HCl/C–HO/O–HS hydrogen bonds [average d(DA) = 3.501 (Å)] between a metal–organic unit and chloride– water molecules (Table 1) lead to the formation of a 3D supramolecular framework. The selected hydrogen bonding parameters are given in Table 1. The different chloride anions are strongly held in lattice by O–HCl and C–HCl hydrogen bonds (Fig. S7, ESI†), Cl1 is held between three nearby water molecules [O1–H1Cl1 = 3.121 Å, O3–H3Cl1 = 3.148 Å and O4–H4Cl2 = 3.056 Å]. Similar hydrogen bonding is also observed for Cl2 [O5–H5Cl2 = 3.066 Å and O10–H10Cl2 = 3.066 Å]. The ClO separations are smaller than those previously reported for Cl(H2O)4 52 and Cl2(H2O) OO distances are in the range from 2.711 to 2.863 Å with an average value of 2.79 Å, which can be compared with OO distances of 2.76 Å in hexagonal (Ih) ice (at 200 K),55 2.74 Å in cubic (Ic) ice56 or 2.85 Å in liquid water.57 OOO angles vary from 102.25 to 124.271 with an average of 112.71 which slightly deviated from the angle of 109.31 on hexagonal ice.55 Seven of ten water molecules participative in the formation of three hydrogen bonds each (accepting one hydrogen and donating two), while the O2, O7, and O10 water molecules along with Cl1 and Cl2 are involved in four hydrogen bonding contacts. The different cyclic fragments in the 2D network (Fig. 2c) are classified in Table 2. Altogether there are six different cycles, that is two tetra-nuclear, one penta-nuclear, two hexa-nuclear and one-dodeca nuclear fragments (Fig. 2c and Table 2). One of them contains only water molecules, while other five rings are chloride–water hybrids with one or two or four chloride atoms. The lengthy OO or ClCl non-bonding separations within the fragments vary from 4.449 to 14.307 Å (Table 2).

Moreover, the present finding extends the still limited number48–51 of the well-characterized examples of large polymeric 2D water–chloride assemblies intercalated in crystalline materials and shows that [1,2,5]-thiadiazolo-[3,4-f]-[1,10]-phenanthroline (tdzp) complexes can offer rather appropriate matrixes to stabilize and store water–chloride clusters. Further work is currently under progress aiming to get more information about how the modification of the [1,2,5]-thiadiazolo-[3,4-f]-[1,10]- phenanthroline (tdzp) ligand or the replacement of chlorides by

International journal of basic and applied research
www.pragatipublication.com
ISSN 2249-3352 (P) 2278-0505 (E)
Cosmos Impact Factor-5.86

other counter ions with a high accepting capacity toward

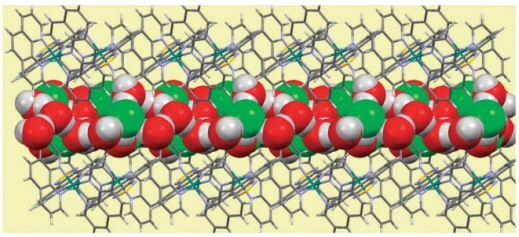

Fig. 3 Crystal packing diagram space fill model showing water–chlorine water channels along the 'c' axis.

Table 2 Description of cyclic fragments within the water–chloride network in **2**

Cycle number	Number of O/Cl atoms	Formula	Atom numbering scheme	Geometry	Most lengthy non-bonding separation (Å)
1	4	$[(H_2O)_2(Cl)]^-$	O_2–O_2–O_4–Cl_1	Planar	$O_2\cdots Cl_1$, 4.449
2	4	$[(H_2O)_2(Cl)_2]^{2-}$	O_4–Cl_1–O_4–Cl_1	Planar/non-planar	$Cl_1\cdots Cl_1$,4.707
3	5	$[(H_2O)_2(Cl)]^-$	O_4–O_4–O_4–O_2–Cl_1	Non-planar	$O_2\cdots O_4$, 4.712
4	6	$[(H_2O)_3]$	O_2–O_2–O_2–O_4–O_2	Planar	$O_2\cdots O_2$, 6.282
5	6	$[(H_2O)_2(Cl)]^-$	O_2–O_2–O_4–O_4–O_{10}–Cl_2	Non-planar	$O_2\cdots O_{10}$, 5.802
6	12	$[(H_2O)_6(Cl)_6]^{4-}$	O_2–O_2–Cl_2–O_2–O_4–Cl_1–O_2–O_2–Cl_2–O_2–O_4–Cl_1	Non-planar	$Cl_1\cdots Cl_1$, 14.309

hydrogen-bonds can affect the type and topology of the hybrid water containing associates within various [1,2,5]-thiadiazolo- [3,4-f]-[1,10]-phenanthroline (tdzp) transition metal complexes. Further the reversible dehydration and rehydration process in 2 was monitored by observing the changes in intensity of the infrared band corresponding to water in the FT-IR spectra of parent, dehydrated, and rehydrated samples. The water molecules from the crystal lattice were removed by heating the sample at 230 1C for 2 h. The comparative IR spectra of the parent crystalline solid of 2, dehydrated solid and rehydrated solid are given in Fig. S9, ESI.† The IR spectrum of parent 2 shows a broad band centred at around 3380 cm1 assigned to the O–H stretching frequency of the water cluster (Fig. S9, ESI†). The intensity of this band decreases significantly upon heating the parent sample at 230 1C for 2 h, suggesting the escape of water molecules. The exposing of the dehydrated sample of 2 to moisture overnight showed the reappearance of the band at 3382 cm1 . This result strongly suggests that dehydrated 2 is reversible in the solid state with reabsorption of the water molecule.

Photophysical properties

The absorption and emission spectra of complexes 1–3 are given in Fig. 4, and photophysical properties of complexes 1–3 in different solvents are summarized in Table 3. The absorption spectra of complexes 1–3 (Fig. 4) are dominated by high-energy bands between 240 to 340 nm which are related to the p - p* transitions of the aromatic nitrogen donor ligands.43,58,59 The band around 450 nm for complexes 1–3 is assigned as the MLCT Ru (dp) - ligand (p*) transitions typical of polypyridyl ruthenium(II) complexes.

The emission spectra of complexes 1–3 recorded in various solvents by excitation of the MLCT band at room temperature shows a characteristic broad emission peak at around 550– 750 nm (Fig. 4). The emission maxima, relative quantum yield in different solvents are given in Table 3. All complexes show solvent dependent properties and are highly luminescent. The emission quantum yield of complexes 1–3 in methanol and DMF is higher than that of [Ru(bpy)3] 2+.

DNA interaction studies

Before carringout DNA binding studies, the stability of complexes in water was checked by comparing the UV-Visible spectra of complexes recorded immediatly after dissolving in water and after 8th day of dissolving (Fig. S10, ESI†). The spectra show no obvious changes confirming the stability of these complexes in water.

International journal of basic and applied research
www.pragatipublication.com
ISSN 2249-3352 (P) 2278-0505 (E)
Cosmos Impact Factor-5.86

Absorption titration

Electronic absorption spectroscopy is one of the most widely used techniques for exploring the interaction of metal complexes with DNA.21,31–36 Strong interaction of complex with DNA through

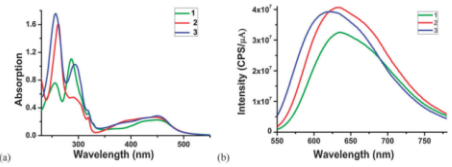

Fig. 4 Absorption (left) and emission (right) spectra of 1–3 in methanol (20 mM).

Table 3 UV/Vis and emission data for complexes 1–3

	Absorbance λ_{max} (nm)/ε (M^{-1} cm^{-1})		Emission					
	Methanol		Methanol		DMF		Water	
Complex[a]	Ligand transitions	MLCT	λ_{em}[c]/nm	ϕ_{em}[d]	λ_{em}[c]/nm	ϕ_{em}[d]	λ_{em}[c]/nm	ϕ_{em}[d]
1	256/38 100 286/55 800 319/16 300	450/11 300	635	0.052	643	0.091	637	0.014
2	262/81 100 292/27 800 319/13 100	448/13 000	629	0.058	646	0.102	636	0.031
3	256/88 300 294/51 400 318/18 500	452/14 200	622	0.052	637	0.094	637	0.043
$[Ru(bpy)_3]^{2+}$[b]	—		630	0.045	629	0.063	630	0.042

[a] [Ru] = 20 (±0.2) μM. [b] Data taken from ref. 60. [c] Emission maxima. [d] ϕ = emission quantum yield, error limit: λ_{max} = ±2 nm, λ_{em} = ±2 nm, ϕ = ±5%.

intercalation leads to hypochromism and a red shift, due to the interaction between the aromatic chromophore of the complex and the base pairs of the DNA.30,61 The amount of hypochromism and red shift depends on the strength of the interaction of the complex with DNA.30–34,61 Changes in absorption spectra of complexes 1–3 with increasing concentration of DNA are shown in Fig. 5 and Fig. S11 (ESI†). The percentage of hypochromism and red shift for complexes 1–3 in the presence of CT-DNA are given in Table 4. The intrinsic binding constant of complexes 1–3 with CT-DNA is calculated using eqn (2) by observing the changes in the MLCT band with increasing concentration of DNA (Fig. 5 and Fig. S11, ESI†). The binding constants are 7.6 103 , 1.05 104 and 1.2 104 M1 for complexes 1–3 respectively. Binding constants for complexes are comparable to that of known DNA intercalators such as 3.9 105 M1 for [Ru(bpy)2(dcdpq)]2+ (dcdpq = dicyano-dipyrido[3,2-d:20 ,30 -f]quinoxaline),62 4.7 104 M1 for [Ru(bpy)2(dpq)]2+, 62 6.3 104 M1 for [Ru(bpy)2- (dpt)]2+ (dpt = 3-(pyrasin-yl)-as-triazino[5,6-f]phenanthrene),

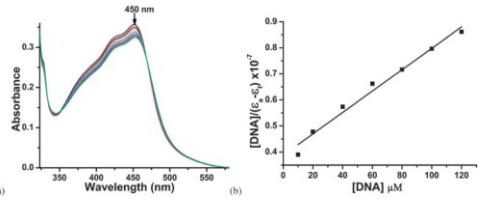

Fig. 5 (a) Changes in the electronic absorption spectra of complex 3 (20 mM), with increasing concentrations of CT-DNA (0–140 mM) (phosphate buffer, pH 7.2), (b) fitting of the absorbance data used to obtain the binding constant.

Table 4 Electronic absorption data upon addition of CT-DNA

Complex[a]	$\Delta\lambda_{max}$ (MLCT)	Hypochromism H[b] (%)			K_b (M^{-1})	Ref.
1	2	4.7 (448)	5.3 (286)	6.8 (256)	7.6×10^3	Present work
2	2	6.8 (450)	10.2 (292)	8.3 (260)	1.05×10^4	Present work
3	4	9.1 (452)	11.8 (294)	13.5 (256)	1.2×10^4	Present work
$[Ru(bpy)_2(dcdpq)]^{2+}$	2	20.0 (450)	—	—	3.9×10^3	62
$[Ru(bpy)_2(dpq)]^{2+}$	5	14.0 (453)	—	—	4.7×10^4	62
$[Ru(bpy)_2(dpt)]^{2+}$	5	18.1 (474)	—	—	6.3×10^4	63
$[Ru(bpy)_2(aip)]^{2+}$	—	—	23.0 (367)	43.0 (253)	4.9×10^3	64

[a] Ru = 20 μM ± 0.5 μM. [b] H% = 100 (A_{free} − A_{bound})/A_{free} in phosphate buffer (pH = 7.2) where, A = absorbance, error limit: λ_{max} = ±2 nm, H (%) = ±5%; K_b (M^{-1}) = ±5%.

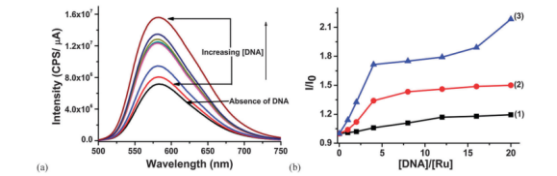

Fig. 6 Emission spectra of complexes (a) 3 (10 mM) in phosphate buffer, pH 7.2, at 298 K with increasing [CT-DNA]/[Ru] ratio 0–20; [complex] = 10 mM, [DNA] = 0–200 mM, (b) plot of relative integrated emission intensity versus [CT-DNA]/[Ru] for the complexes 4.9 0.3 104 M1 for [Ru(bpy)2(aip)]2+ (aip = 2-(9-anthryl)-1Himidazo[4,5-f][1,10]phenanthroline).64 The spectral characteristic as well as Kb value suggests that the complexes 2 and 3 bind to DNA by the partial intercalative mode involving

Index in Cosmos
Sep 2024, Volume 14, ISSUE 3
UGC Approved Journal

International journal of basic and applied research
www.pragatipublication.com
ISSN 2249-3352 (P) 2278-0505 (E)
Cosmos Impact Factor-5.86

stacking interaction between the aromatic chromophore and base pairs of the DNA.

Emission titration

The investigation of changes in luminescence properties of ruthenium complexes in the presence of DNA provides useful information about the type of DNA binding modes.43,65 Changes in emission spectra of complexes (10 mM) in phosphate buffer (pH 7.2) with increasing concentrations of DNA is shown in Fig. 6 and Fig. S12 (ESI†). Complex 1 exhibits very weak enhancement in luminescence intensity after adding CT-DNA indicating weak binding of the complex with DNA by electrostatic interaction. But complexes 2 and 3 show larger enhancement in luminescence intensity indicating strong binding of complexes with DNA either by groove or partial intercalation mode. These results are consistent with that of absorption titration experiments. The increase in luminescence intensity is due to two reasons: firstly, the hydrophobic environment inside the DNA helix reduces the accessibility of water molecules to the complex, and secondly, the complex mobility is restricted at the binding site and so the vibrational mode of relaxation decreases.

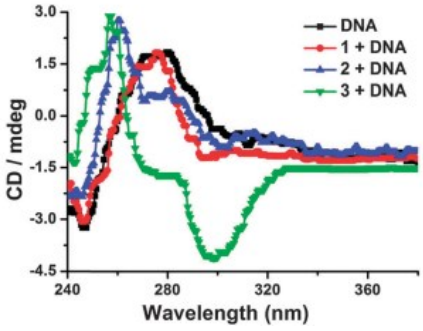

Fig. 7 CD spectra of CT-DNA in the presence and absence of complexes 1–3, in phosphate buffer (pH 7.2), [DNA]/[complex] = 4, [DNA] = 200 mM.

Circular dichroism spectral analysis

CD spectral analysis was used to monitor the conformational changes in DNA as a result of interaction with complexes with DNA.66,67 In CD spectrum of CT-DNA a positive band at 280 nm is assigned to the base pair stacking and band at 245 nm due to the right handed helicity characteristic of B-DNA.68 The CD spectrum of CT-DNA was sensitive to its conformational changes. The absorption and emission titration experiments show interaction of these complexes with DNA, and to further confirm these interactions, circular dichroism (CD) spectra of DNA was recorded in the presence and absence of complexes 1–3. As shown in Fig. 7 in the presence of complex 1 small change in the CD spectrum of DNA was observed due to weak electrostatic interaction of the complex with DNA. In the case of complex 2 increase in the intensity of the positive band at 270 nm along with a blue shift of 18 nm was observed, which may be due to the groove or partial intercalation of complex 2 with DNA (Fig. 7). In presence of complex 3 larger changes in the CD spectrum of DNA was observed, the positive band at 270 nm is blue shifted by 22 nm and large enhancement of negative band intensity at 298 nm (Fig. 7) demonstrating the intercalative mode of binding with DNA

Electrophoretic mobility shift assay

In order to assess any damage of the DNA as a result of binding of these complexes, agarose gel electrophoresis has been performed with a circular form of plasmid pBR322 DNA. DNA cleavage ability of

International journal of basic and applied research
www.pragatipublication.com
ISSN 2249-3352 (P) 2278-0505 (E)
Cosmos Impact Factor-5.86

complexes 1–3 at low concentrations is shown in Fig. 8. Upon incubation of complexes 1–3 with plasmid pBR322 DNA under dark experimental conditions the conversion of super coiled DNA (Form I) into open circular DNA (Form II) was observed, but in the case of complex 3 conversion of supercoiled DNA into open circular as well as linear DNA was observed. At higher complex concentration and incubation time smearing of DNA bands was observed. The higher cleavage activity of complex 3 compared to complexes 1 and 2 is due to its higher DNA binding strength.

Cellular uptake and cytotoxicity studies

The cellular localization of complexes is monitored by fluorescence microscopy. Complexes are highly luminescent upon excitation at

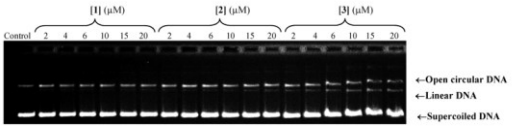

Fig. 8 Agarose (1%) gel electrophoresis of pBR 322 DNA under dark experimental conditions, [complex] = 2–20 mM, [DNA] = 200 ng, incubation time = 15 min, at 37 1C. TBE buffer, pH 8.2.

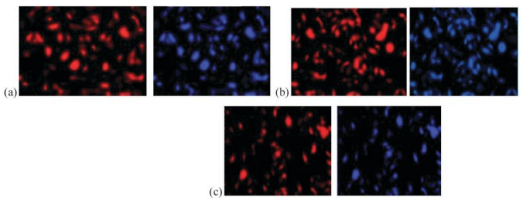

Fig. 9 Fluorescence microscopy images of HeLa cells incubated (48 h) with 15 mM of complexes and co-staining with DNA specific stain DAPI (a) cells incubated with complex 1 (left), DAPI co-staining (right); (b) cells incubated with complex 2 (left), DAPI co-staining (right); (c) cells incubated with complex 3 (left), DAPI co-staining (right).

the MLCT band and clearly visible within the cell after 24 h incubation (Fig. 9). To confirm the accumulation of the ruthenium complexes within the cell, a co-staining experiment with the DNAspecific dye DAPI (DAPI = 40 ,6-diamidino-2-phenylindole) was performed and strong co-localization of two emission signals was observed (Fig. 9), confirming nuclear staining by the complexes. The fluorescence microscopy images of cells clearly show that complexes 1–3 have staining patterns closely resembling to the standard DNA staining dye DAPI.

The in vitro cytotoxicity of complexes 1–3 against a HeLa (cervical) cancer cell line has been tested by MTT [3-(4,5-dimethylthiazol-2-yl)-2,5-diphenyltetrazolium bromide] assay. These complexes exhibit significant cytotoxicity in a concentration dependent manner (Fig. 10). The percent cell viability of HeLa cell lines in the presence of complex 1–3 was measured in the concentration range of 1 mM to 50 mM, the compounds tested were found to be active at lower concentrations. Complexes 1–3 exhibits significant cytotoxicity against the HeLa cell line by inducing apoptosis and can be viewed as potential candidates for antitumor therapy. The IC50 values against HeLa cell line are 28 ——————————
0.12, 21 ——————————
0.08 and 19 ——————————
0.08 mM for complex 1, 2 and 3 respectively. We think that anticancer activity of complexes 1–3 may not be only due to partial intercalation or groove binding, but also due to the specific

International journal of basic and applied research
www.pragatipublication.com
ISSN 2249-3352 (P) 2278-0505 (E)
Cosmos Impact Factor-5.86

chemical structure and the nature of the ligands used.

III. CONCLUSION

In summary, we have synthesized and characterized a series of mononuclear ruthenium(II) polypyridyl complexes 1–3. The molecular structure of complex 2 was confirmed by single crystal X-ray structure determination. We have crystallographically characterized the polymeric cyclic hybrid chloride–water cluster {[(H2O)10(Cl)2] 2}n encapsulated in complex 2. This water–chloride cluster has been trapped by a cationic ruthenium(II) polypyridyl cation, which is stabilized by strong hydrogen bonding interactions between the cationic unit and chloride anions–water molecules. All complexes show solvent dependent photophysical properties. All complexes interact with DNA and the order of binding of the complexes to DNA is 3 4 2 4 1 reflecting that the increase in planarity of ligands plays important role in DNA binding. Fluorescence microscopy studies reveal the nuclear staining by complexes and apoptosis mode of cell death. Notably, 1–3 exhibit potent

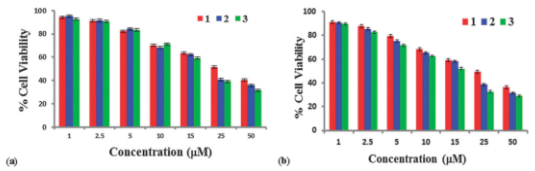

Fig. 10 Concentration dependent cytotoxicity of complexes 1–3 against a HeLa cell line evaluated by MTT assay, (a) after 48 h, (b) after 72 h. Results are mean values of three biological replicates and that in each biological replicate there were four technical replicates.

antiproliferative activities against a panel of human cancer cell lines. Given these properties, analogues of these complexes could be developed as novel agents as probes for the nucleic acid structure.

REFERENCES

1 C. Metcalfe and J. A. Thomas, Chem. Soc. Rev., 2003, 32, 215–224.

2 A. E. Friedman, J. C. Chambron, J. P. Sauvage, N. J. Turro and J. K. Barton, J. Am. Chem. Soc., 1990, 112, 4960–4962.

3 S. Ramakrishnan, E. Suresh, A. Riyasdeen, M. A. Akbarsha and M. Palaniandavar, Dalton Trans., 2011, 40, 3524–3536.

4 M. R. Gill and J. A. Thomas, Chem. Soc. Rev., 2012, 41, 3179–3192.

5 Q. Zhao, C. Huang and F. Li, Chem. Soc. Rev., 2011, 40, 2508–2524.

6 G. Liao, X. Chen, J. Wu, C. Qian, H. Wang, L. Ji and H. Chao, Dalton Trans., 2014, 43, 7811–7819.

7 Z. Zhu, L. Xu, H. Li, X. Zhou, J. Qin and C. Yang, Chem. Commun., 2014, 50, 7060–7062.

8 C. Santini, M. Pellei, V. Gandin, M. Porchia, F. Tisato and C. Marzano, Chem. Rev., 2014, 114, 815–862.

9 M.-J. Li, T.-Y. Lan, X.-H. Cao, H.-H. Yang, Y. Shi, C. Yi and G.-N. Chen, Dalton Trans., 2014, 43, 2789–2798.

10 S. P. Dash, A. K. Panda, S. Pasayat, R. Dinda, A. Biswas, E. R. T. Tiekink, Y. P. Patil, M. Nethaji, W. Kaminsky, S. Mukhopadhyay and S. K. Bhutia, Dalton Trans., 2014, 43, 10139–10156.

International journal of basic and applied research
www.pragatipublication.com
ISSN 2249-3352 (P) 2278-0505 (E)
Cosmos Impact Factor-5.86

11 X.-B. Fu, D.-D. Liu, Y. Lin, W. Hu, Z.-W. Mao and X.-Y. Le, Dalton Trans., 2014, 43, 8721–8737.

12 B. Pen˜a, A. David, C. Pavani, M. S. Baptista, J.-P. Pellois, C. Turro and K. R. Dunbar, Organometallics, 2014, 33, 1100–1103.

13 B. Elias and A. K.-D. Mesmaeker, Coord. Chem. Rev., 2006, 250, 1627–1641.

14 J. G. Vos and J. M. Kelly, Dalton Trans., 2006, 4869–4883.

15 N. J. Turro, J. K. Barton and A. T. Donald, Acc. Chem. Res., 1991, 24, 332–340.